REDVET - Revista electrónica de Veterinaria - ISSN 1695-7504
Vol 25, No. 01 (2024)
http://www.veterinaria.org
Received 07 April 2024 Revised 13 May 2024 Accepted 20 June 2024

Deciphering the Molecular Mechanism of *Butea monosperma* Flowers Against Cervical Cancer: An Integrated Network Pharmacology, Molecular Docking, and MD Simulation Approach

Suresh Kumar Gopal[1]*, Rakesh Kumar Jatt[2], Abdul Mannan Khan[3]

[1]*Research Scholar, Department of Pharmaceutical Sciences, Shri Jagdishprasad Jhabarmal Tibrewala University, Vidyanagari, Jhunjhunu Churu Road, Chudela, District - Jhunjhunu Rajasthan – 333010. Mobile no: 9384266716; e-mail ID: Sureshbiotech1983@gmail.com. ORCID ID: 0009-0004-5034-0166
[2] Director-cum-Principal, Department of Pharmacy, Shri Jagdishprasad Jhabarmal Tibrewala University, Vidyanagari, Jhunjhunu Churu Road, Chudela, District - Jhunjhunu Rajasthan – 333010. Mobile no: 9667212243; e-mail ID: pharmacy@jjtu.ac.in.
[3] Professor, Department of Pharmacy, Shri Jagdishprasad Jhabarmal Tibrewala University, Vidyanagari, Jhunjhunu Churu Road, Chudela, District - Jhunjhunu Rajasthan – 333010. Mobile no: 9571063360; e-mail ID - drmannan.bux@gmail.com

Abstract
Cervical cancer remains a critical global health challenge, ranking as the fourth leading cause of cancer-related mortality among women, particularly in low-resource regions. Because conventional treatments are often limited by low efficacy and adverse off-target effects, there is a pressing need to discover multi-targeted therapeutic agents from natural sources. This study utilizes an integrated approach—combining systems pharmacology, molecular docking, and molecular dynamics simulations—to elucidate the anti-cancer potential of *Butea monosperma* Taub. flowers.
Through extensive database screening, 21 phytochemical constituents were identified, of which six compounds demonstrated optimal pharmacokinetic profiles and strict adherence to drug-likeness filters. A multi-layered network analysis revealed 598 common targets between *B. monosperma* and cervical cancer, identifying ten core hub genes: TP53, EGFR, SRC, HSP90AA1, STAT3, AKT1, TNF, HSP90AB1, BCL2, and HIF1A. Molecular docking analysis demonstrated high binding affinities, with Isobutrin showing superior potential against SRC, Monospermoside against AKT1, and Coreopsin against EGFR.
Functional enrichment through GO and KEGG pathways indicated that these phytochemicals primarily modulate the PI3K/AKT/mTOR and IL-6/STAT3 signaling axes to induce apoptosis and cell cycle arrest. MD simulations further validated the thermodynamic stability of these protein-ligand interactions, yielding low eigenvalues and significant rigidification of the binding pockets. These findings provide a rigorous computational foundation for using *B. monosperma* flowers as a source of potent, multi-targeted inhibitors for the management of cervical malignancy

Keywords: *Butea monosperma*, Cervical Cancer, Network Pharmacology, Molecular Docking, Molecular Dynamics Simulations, Hub Genes, Apoptosis.

1.Introduction

Cervical cancer remains a significant cause of morbidity and mortality among women worldwide, marked by stark geographic and socioeconomic disparities (2). Recent multidimensional analyses using global health data indicate that incident cases and deaths remain high, with regions like Sub-Saharan Africa bearing a heavy burden (1,11). In most countries, incidence and mortality rates remain significantly higher than the threshold set by the WHO Global Cervical Cancer Elimination Initiative, which aims to reduce the age-standardized incidence to below 4 per 100,000 women-years (11). This disparity is driven by limited access to HPV screening and vaccination in low- and middle-income countries, where rural residence and low education levels further compound health system challenges (2).
Traditional drug discovery often relies on a "one-drug, one-target" strategy, which may lack efficacy and carry significant side effects in the treatment of complex, multifactorial diseases like cervical cancer (12). Consequently, there is an urgent need to identify biologically active ingredients from traditional medicine using systems biology approaches (12). Network pharmacology offers a holistic perspective by unraveling the relationship between plant-derived compounds and cancer-associated protein networks (12,13). This methodology is increasingly used to identify core targets—such as those involved in cell cycle regulation and apoptosis—thereby providing an innovative platform for discovering multi-targeted combination therapies (6,13).
Butea monosperma, known as "Palash" or "Flame of the Forest," has a long history of use in Ayurvedic medicine for treating various ailments, including abdominal tumors and inflammation (5). The flowers are particularly rich in bioactive flavonoids and chalcones, such as butein, butrin, and isobutrin (5,14). These compounds have demonstrated significant chemopreventive effects by suppressing tumor progression and inducing apoptosis in various malignancies (9,15). Specifically, butein has been shown to down-regulate oncogenic signaling pathways and generate reactive oxygen species to trigger cell death in cancerous cells (9,16). Despite these findings, there is a persistent need to further validate the

REDVET - Revista electrónica de Veterinaria - ISSN 1695-7504
Vol 25, No. 01 (2024)
http://www.veterinaria.org
Received 07 April 2024 Revised 13 May 2024 Accepted 20 June 2024

molecular mechanisms of *B. monosperma* flowers using modern computational tools to facilitate its development into a modern therapeutic option (4,7).

2. Methodology

2.1 Identification and Selection of Bioactive Compounds

The bioactive phytochemicals of *Butea monosperma* flowers were identified through a systematic search of the IMPPAT database and a comprehensive review of existing pharmacological literature (6,14). The search prioritized key constituents such as butein, butrin, and isobutrin, which have documented roles in modulating oncogenic signaling (6,15). Canonical SMILES strings and 3D structures were retrieved from PubChem to facilitate structural optimization and subsequent docking analyses (7).

2.2 Pharmacokinetic Screening and Drug-likeness Evaluation

To evaluate the therapeutic viability of the identified constituents, we conducted an ADME analysis using the SwissADME server (5,14). Each compound was filtered based on Lipinski's Rule of Five and Veber's criteria (rotatable bonds $\leq$ 10 and TPSA $\leq$140 Å^2) to ensure drug-likeness and oral bioavailability (4,7). Key parameters, including gastrointestinal absorption and P-glycoprotein substrate status, were assessed to prioritize compounds with favorable pharmacological profiles (4,5).

2.3 Acquisition of Disease Targets and Differential Expression Analysis

Cervical cancer-related transcriptomic data were retrieved from the NCBI Gene Expression Omnibus, specifically focusing on datasets GSE9750, GSE138080, and GSE7803 (8). Differentially expressed genes were identified using a significance threshold of $p < 0.05$ and $|\log_2 FC| \geq 1$. To build a comprehensive disease-target library, these genes were intersected with data from GeneCards, OMIM, and Malacards, ensuring a robust representation of the disease interactome (8,13).

2.4 Protein-Protein Interaction Network and Hub Gene Identification

To visualize the interactome between phytochemical targets and cervical cancer-related genes, a PPI network was constructed using the STRING database (3). The analysis was restricted to *Homo sapiens* with a high-confidence interaction score ($\geq$0.7) to minimize false positives (3,8). The network was then analyzed in Cytoscape 3.9.1, where the CytoHubba plugin was employed to rank proteins based on topological metrics such as degree centrality and betweenness. The top 10 genes were designated as "hub genes" for further investigation (3,8).

2.5 Functional Enrichment and Pathway Analysis

To elucidate the molecular mechanisms of *B. monosperma*, Gene Ontology and Kyoto Encyclopedia of Genes and Genomes pathway enrichment analyses were performed using ShinyGO 0.7 (8). Target genes were mapped to specific biological processes, including the regulation of apoptosis and the modulation of key oncogenic axes such as the PI3K/AKT/mTOR and IL-6/STAT3/FoxO3a pathways (9,10).

2.6 Clinical Validation and Survival Analysis

The expression levels and prognostic significance of the identified hub genes were validated using the GEPIA database, which integrates data from TCGA and GTEx (8). This allowed for a comparison of gene expression between tumor and normal tissues and the generation of Kaplan-Meier survival curves to assess the clinical relevance of target proteins in cervical squamous cell carcinoma and adenocarcinoma (8).

2.7 Molecular Docking Simulations

To investigate the binding affinity and specific interaction modes between the *Butea monosperma* phytochemicals and the prioritized hub proteins, molecular docking simulations were conducted using AutoDock Vina integrated within the UCSF Chimera interface (5,7). The three-dimensional crystal structures of the target proteins, including AKT1 (PDB ID: 4GTK), EGFR (PDB ID: 1XKK), and SRC (PDB ID: 2H8H), were retrieved from the Protein Data Bank (3,7). Protein preparation involved the removal of co-crystallized water molecules and heteroatoms, the addition of polar hydrogen atoms, and the assignment of **G**asteiger charge**s** to ensure accurate electrostatic modeling (3,7).

The ligands were similarly prepared and subjected to energy minimization to achieve their most stable conformations prior to docking. The docking grid boxes were centered on the known active sites or the coordinates of co-crystallized inhibitors to ensure site-specific binding (5,7). Binding affinities were recorded in kcal/mol, where a lower (more negative) energy score indicates a more stable protein-ligand complex (5,7). Finally, the resulting docking poses and molecular interactions—including hydrogen bonding, hydrophobic contacts, and pi-stacking—were visualized and analyzed using BIOVIA Discovery Studio Visualizer and UCSF Chimera to elucidate the structural basis of the inhibition (3,5).

2.8 Molecular Dynamics Simulations and Complex Stability

REDVET - Revista electrónica de Veterinaria - ISSN 1695-7504
Vol 25, No. 01 (2024)
http://www.veterinaria.org
Received 07 April 2024 Revised 13 May 2024 Accepted 20 June 2024

The thermodynamic stability and flexibility of the prioritized protein-ligand complexes were validated through Normal Mode Analysis and residue-level fluctuation assessments (5,12). The CABS-flex 2.0 platform was used to determine the Root Mean Square Fluctuation of the bound state (17). Additionally, the iMODS server was utilized to evaluate collective dynamics, focusing on parameters such as deformability, eigenvalues, and variance to ensure structural integrity under physiological-like conditions (5,17).
The thermodynamic stability and flexibility of the prioritized protein-ligand complexes were validated through Molecular Dynamics simulations (5). Residue-level fluctuations were assessed using the CABS-flex 2.0 platform to determine the Root Mean Square Fluctuation of the bound state relative to the apo-protein (17). Furthermore, the iMODS server was utilized for Normal Mode Analysis to evaluate the collective dynamics of the complexes. We focused on parameters such as deformability, eigenvalues, and variance to ensure structural integrity and the maintenance of a stable binding pose under physiological-like conditions (5,17).

3. Results

3.1 Physicochemical and ADME Analysis of *Butea monosperma* Compounds

Based on literature mining and network pharmacology principles, 21 phytochemical constituents of *Butea monosperma* flowers were screened and analyzed using the SwissADME server to evaluate their physicochemical properties, pharmacokinetics, and drug-likeness profiles (14), was shown in Table 3.1. The bioactive compounds identified in this study exhibited molecular weights ranging from 146.14 g/mol to 596.53 g/mol, with flavonoid-based constituents generally displaying moderate lipophilicity, which supports aqueous solubility and passive membrane diffusion. However, larger glycosylated flavonoids, such as Palasitrin, Butrin, and Isobutrin, exceeded the 500 Da threshold, potentially limiting their membrane permeability. Analysis of LogP values, which varied significantly from –1.71 to 8.1, alongside BOILED-Egg plots, suggested that most compounds possess moderate Topological Polar Surface Areas and partition coefficients conducive to favorable bioavailability. Notably, butein, butin, formononetin, and afrormosin demonstrated high gastrointestinal absorption; specifically, butein has been identified as a key lead because it suppresses cervical cancer growth by modulating the PI3K/AKT/mTOR pathway (9). In contrast, glycosylated derivatives like Isobutrin and Butrin exhibited poor GI absorption due to high TPSA values (>140 Å²) and the presence of polar functional groups. While most constituents were not identified as substrates for P-glycoprotein, Coreopsin and Isomonospermoside were found to be substrates, suggesting a susceptibility to efflux-mediated loss. Ultimately, six compounds—Butein, Butin, Isoliquiritigenin, Liquiritigenin, Formononetin, and Afrormosin—successfully adhered to major drug-likeness filters, achieving a bioavailability score of 0.55 without PAINS or Brenk structural alerts, confirming their potential as therapeutic candidates for further investigation.

Table 3.1: ADME properties of the selected bioactive compounds of *Butea monosperma* flowers

S.No	Name of the Compound	Molecular weight (g/mol)	Molar Refractivity	Num. rotatable bonds	XLOGP3	Num. H-bond acceptors	Num. H-bond donors	Bioavailability Score
1	Tetracosanoic acid	368.64	119.25	22	11.46	2	1	0.85
2	Coreopsin	434.39	106.46	6	1.02	10	7	0.55
3	Isomonospermoside	434.39	103.69	4	0.14	10	6	0.55
4	Palasitrin	594.52	136.13	7	-1.08	15	9	0.17
5	Monospermoside	434.39	106.46	6	1.02	10	7	0.55
6	Coumarin	146.14	42.48	0	1.39	2	0	0.55
7	Stearic acid	284.48	90.41	16	8.23	2	1	0.85
8	Butein	272.25	74.34	3	2.82	5	4	0.55
9	Isobutrin	596.53	138.58	9	-0.79	15	10	0.17
10	Butrin	596.53	135.81	7	-1.67	15	9	0.17
11	Palmitic acid	256.42	80.8	14	7.17	2	1	0.85
12	Butin	272.25	71.57	1	1.94	5	3	0.55
13	Isocoreopsin	434.39	103.69	4	0.14	10	6	0.55
14	Sulfurein	432.38	104.01	4	0.73	10	6	0.55
15	Arachidic acid	312.53	100.03	18	9.29	2	1	0.85
16	beta-Sitosterol	414.71	133.23	6	9.34	1	1	0.55
17	D-Glucose	180.16	35.74	1	-3.24	6	5	0.55
18	D-Fructose	180.16	35.77	1	-2.84	6	5	0.55
19	Dihydromonospermoside	434.39	106.46	6	1.02	10	7	0.55
20	Isoliquiritigenin	256.25	72.32	3	3.18	4	3	0.55
21	7,3',4'-trihydroxyflavone	270.24	73.99	1	2.91	5	3	0.55

REDVET - Revista electrónica de Veterinaria - ISSN 1695-7504
Vol 25, No. 01 (2024)
http://www.veterinaria.org
Received 07 April 2024 Revised 13 May 2024 Accepted 20 June 2024

22	Isomonospermoside	434.39	103.69	4	0.14	10	6	0.55
23	Liquiritigenin	256.25	69.55	1	2.3	4	2	0.55
24	Formononetin	268.26	76.43	2	2.8	4	1	0.55
25	Afrormosin	298.29	82.93	3	2.77	5	1	0.55
26	Formononetin-7-O-Beta-D-Glucopyranoside	430.40	108.56	5	0.99	9	4	0.55
27	Butrin	596.53	135.81	7	-1.67	15	9	0.17
28	Isobutrin	596.53	138.58	9	-0.79	15	10	0.17

3.2 Identification of Potential Targets and Intersection Analysis

To elucidate the multi-targeted mechanism of *B. monosperma* flowers, the 21 screened bioactive compounds were subjected to target prediction analysis using Swiss Target Prediction, which yielded a total of 655 potential protein targets (3,5). Concurrently, a robust library of cervical cancer-associated genes was constructed by integrated mining of the Gene Expression Omnibus—specifically datasets GSE9750, GSE138080, and GSE7803—alongside the MalaCards, OMIM, and GeneCards databases (3,4).

A comprehensive pool of 15,896 target genes associated with cervical cancer was retrieved. To identify the specific points of therapeutic intervention, an overlap analysis between the plant-derived targets and the disease-related genes was performed using Venny 2.1.0 software, resulting in the identification of 598 common targets (4,5), as illustrated in Fig 3.1. These overlapping genes represent the core "therapeutic targets" where *B. monosperma* phytochemicals are likely to exert their anti-cancer effects (4,13). This systematic mapping aligns with core network pharmacology principles, shifting the focus from single-target inhibition to the holistic modulation of complex signaling pathways—such as PI3K/AKT/mTOR and IL-6/STAT3—which are critical for cervical cancer cell survival, proliferation, and metastasis (9,13).

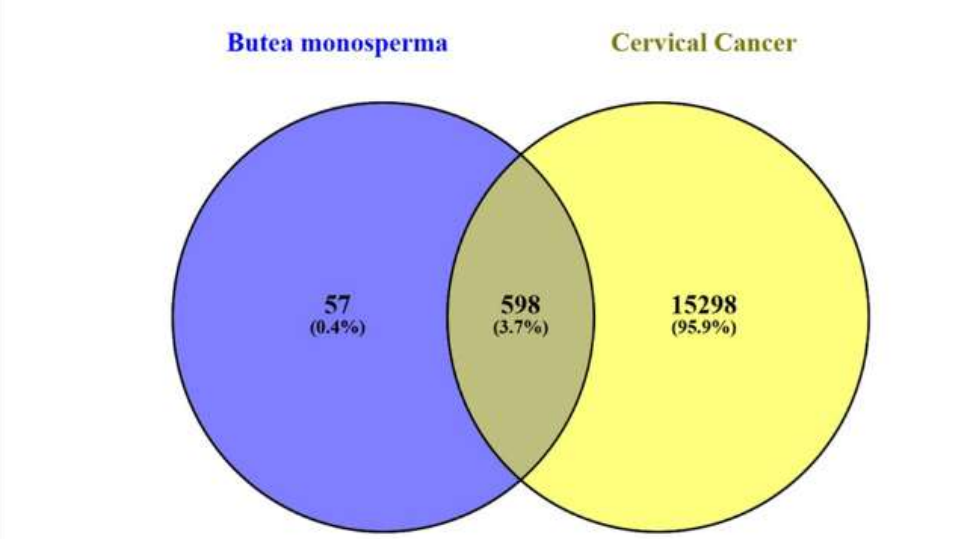

Fig 3.1. Intersecting Targets Between Active Phytochemical Protein Targets of *B.monosperma* flowers and Cervical Cancer–Related Genes

3.3 Construction and Analysis of the Protein-Protein Interaction Network

To elucidate the complex interactome between *Butea monosperma* flower bioactive constituents and cervical cancer targets, a Protein-Protein Interaction network was constructed using the STRING database, specifically targeting *Homo sapiens* proteins where circular nodes represent protein targets and connecting edges indicate functional interaction confidence (5,12), and the results are presented in Fig 3.2. This interactome was visualized in Cytoscape 3.9.1 to assess the topological significance of individual genes, while the most critical regulatory nodes were identified through topological analysis using the cytoHubba plugin (12,13). Applying ranking algorithms based on degree connectivity, the top 10 hub genes were identified as TP53, EGFR, SRC, HSP90AA1, STAT3, AKT1, TNF, HSP90AB1, BCL2, and HIF1A (7,12), as shown in Table 3.2 and Fig 3.3. The centrality of STAT3 and AKT1 is particularly significant, as butein has been shown to suppress cervical cancer growth by modulating the IL-6/STAT3 and PI3K/AKT/mTOR signaling axes to induce apoptosis and cell cycle arrest (9,13). Additionally, the inclusion of BCL2 as a hub gene suggests that *B. monosperma* phytochemicals can trigger programmed cell death by altering the critical Bax/Bcl-2 ratio (9). The resulting hub gene network consists of 10 nodes and 43 edges with a high connectivity of 8.6 neighbors per node, where darker red nodes highlight the primary regulatory targets (12,13). This multi-targeted approach confirms the polypharmacological

REDVET - Revista electrónica de Veterinaria - ISSN 1695-7504
Vol 25, No. 01 (2024)
http://www.veterinaria.org
Received 07 April 2024 Revised 13 May 2024 Accepted 20 June 2024

potential of *B. monosperma* flowers in modulating the dysregulated protein networks characteristic of cervical malignancy (12,13).

.

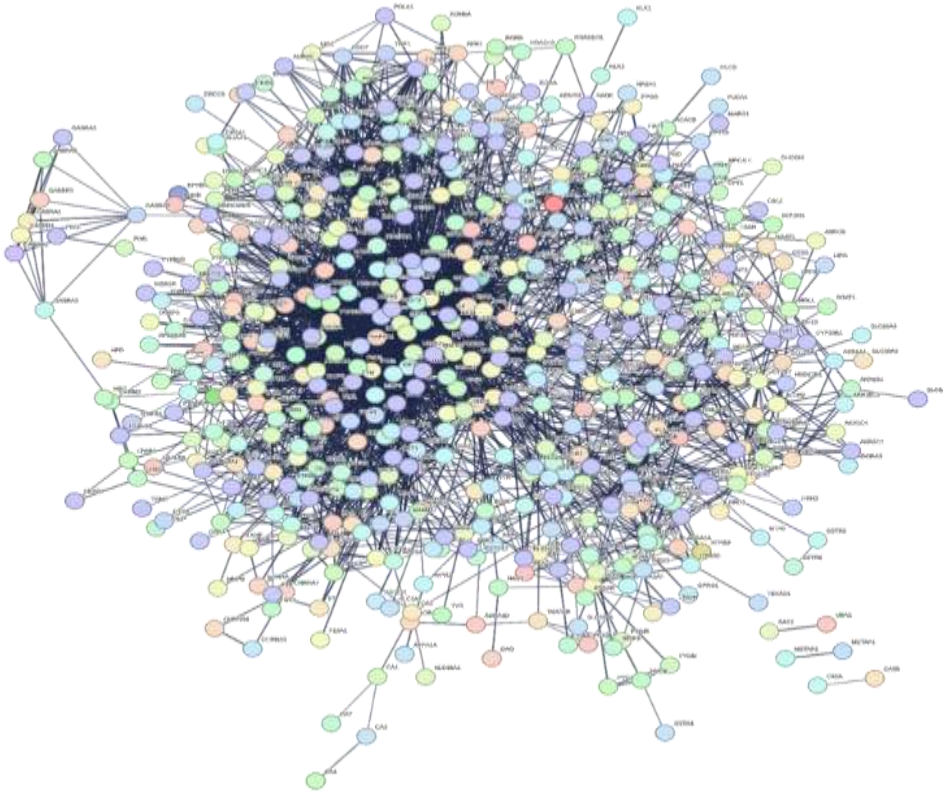

Fig 3.2. Protein-protein interaction (PPI) network of potential targets for *B. monosperma* flowers in the treatment of Cervical Cancer (CC)

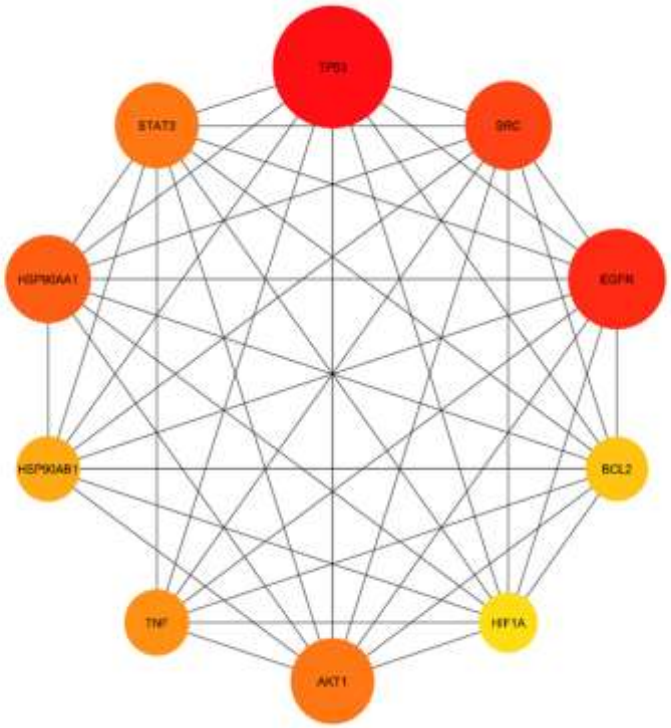

Fig 3.3. Identification and ranking of Key Hub Genes in the Network Module Using CytoHubba in Cytoscape

REDVET - Revista electrónica de Veterinaria - ISSN 1695-7504
Vol 25, No. 01 (2024)
http://www.veterinaria.org
Received 07 April 2024 Revised 13 May 2024 Accepted 20 June 2024

Table 3.2: The degree centrality (DC), betweenness centrality (BC), and closeness centrality (CC) values of the hub genes

Gene	Degree	Betweenness	Closeness
TP53	120	0.109186	0.460199
EGFR	98	0.064801	0.457543
SRC	87	0.06551	0.442231
HSP90AA1	86	0.041569	0.440476
STAT3	84	0.035439	0.433255
AKT1	84	0.056643	0.458678
TNF	65	0.045212	0.428903
HSP90AB1	64	0.015613	0.410503
BCL2	63	0.024167	0.42594
HIF1A	59	0.032566	0.420455

3.4 Construction and Analysis of the Compound-Target-Disease Network

To visualize the complex interplay between the phytochemical constituents of *Butea monosperma* flowers, their respective protein targets, and associated disease pathways, a Compound-Target-Disease network was constructed using Cytoscape, illustrated in Fig 3.4. This network facilitates a polypharmacological understanding of how multiple compounds simultaneously modulate various targets to achieve a therapeutic effect (13,14). The resulting C-T-D network consists of 91 nodes and 163 edges, with an average neighbor size of 2.3.

Topological analysis was employed to identify the most influential bioactive compounds within the network based on their degree centrality, betweenness centrality, and closeness centrality, was displayed in Table 3.3 (14). Among the 21 screened phytochemicals, formononetin, afrormosin, butin, coumarin, monospermoside, and coreopsin emerged as the most significant, exhibiting high degree values ranging from 3 to 4. These high-degree nodes represent "multi-target" compounds that are central to the plant's efficacy against cervical cancer, aligning with the "one-drug/multiple-target" paradigm of network pharmacology (10,13).

Table 3.3: The degree centrality (DC), betweenness centrality (BC), and closeness centrality (CC) values of compounds exhibiting high node degrees

Compounds	Degree	Betweenness	Closeness
Monospermoside	100	0.054376	0.378659
Palmitic acid	100	0.06984	0.378659
7,3',4'-trihydroxyflavone	100	0.060919	0.378659
Coumarin	99	0.140611	0.378197
Tetracosanoic acid	98	0.078399	0.377737

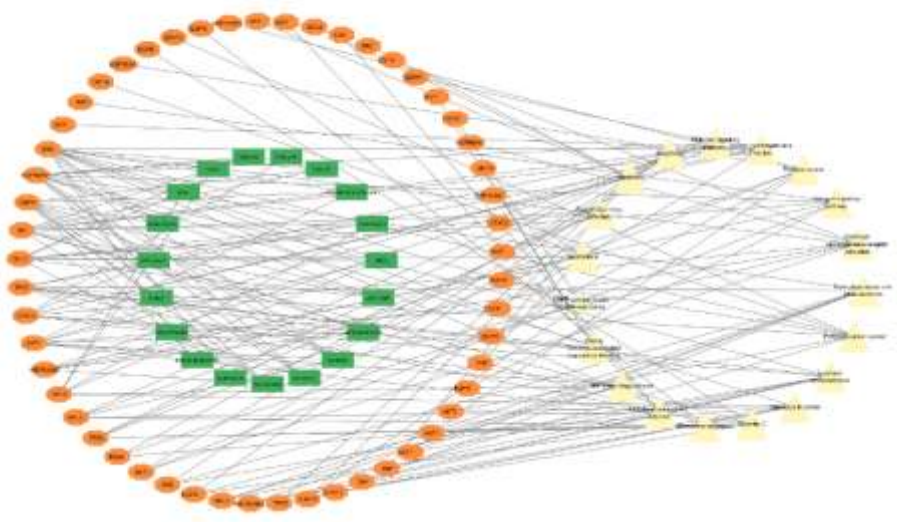

Fig 3.4. Compound-target-pathway network diagram. The green colour represents the compound, orange colour represents the target, and pale yellow represents the path.

REDVET - Revista electrónica de Veterinaria - ISSN 1695-7504
Vol 25, No. 01 (2024)
http://www.veterinaria.org
Received 07 April 2024 Revised 13 May 2024 Accepted 20 June 2024

3.5 Gene Ontology and KEGG Pathway Enrichment Analysis

To elucidate the biological mechanisms through which *B. monosperma* flowers exerts its anti-cancer effects, functional annotation and enrichment analyses were performed. Gene Ontology analysis revealed that the targets are primarily involved in critical biological processes, including cellular responses to endogenous stimuli, protein phosphorylation, homeostatic processes, cell communication, and signal transduction (15). In terms of cellular components, the targets were significantly associated with the plasma membrane, synaptic membrane, cell junctions, and projections. Furthermore, molecular function enrichment highlighted activities such as protein serine/threonine/tyrosine kinase activity, which is pivotal in regulating the oncogenic signaling cascades often dysregulated in cervical malignancy (11,15).

All enrichment results were filtered using a False Discovery Rate threshold of 0.05. Complementary KEGG pathway analysis identified that these targets are predominantly involved in pathways associated with EGFR tyrosine kinase inhibitor resistance, prostate cancer, Kaposi-sarcoma-associated herpes virus infections, and various core cancer-related signaling pathways (10,13). Specifically, the modulation of these pathways by constituents like butein has been shown to inhibit cell growth by blocking the IL-6/STAT3 axis and suppressing the PI3K/AKT/mTOR pathway, thereby inducing apoptosis and G2/M phase arrest in cervical cancer cells (11,15). These findings underscore the multi-targeted curative potential of *B. monosperma* flowers as identified through integrated omics and systems pharmacology approaches (13). The results of GO and KEGG pathway are illustrated in Fig 3.5.

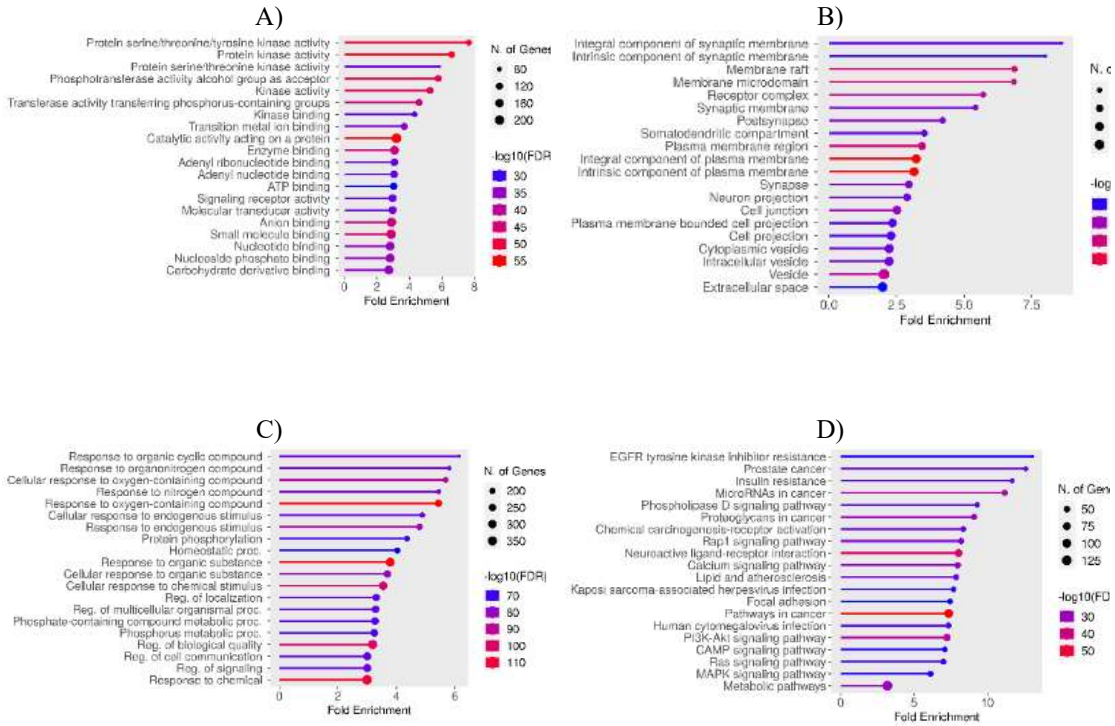

Fig 3.5. The top 20 Gene Ontology (GO) terms and Kyoto Encyclopedia of Genes and Genomes (KEGG) pathways associated with *B. monosperma* flowers and cervical cancer are categorized as follows: A) Molecular Functions, B) Cellular Components, C) Biological Processes, and D) KEGG Pathways.

3.6 Survival Analysis

Prognostic impact analysis helps identify genes linked with favourable or unfavourable survival outcomes and facilitates the identification of potential biomarkers for prognosis and therapeutic targeting in cervical cancer. Kaplan-Meier survival analysis showed that the selected genes exhibited different concentrations in the overall survival of patients with cervical cancer, with statistical significance examined at a p-value threshold of 0.05. High AKT1 expression was not significantly associated with overall survival (HR = 1.1; P = 0.63), facilitating a minimal impact on patient prognosis. Similarly, SRC expression showed no prognostic relevance (HR = 1.0; P = 0.93), indicating a neutral role in the survival outcomes.

Furthermore, the expression levels of STAT3 (HR = 0.99; P = 0.97) and TP53 (HR = 0.99; P = 0.96) were not significantly associated with the overall survival, implying that these genes do not significantly affect the prognosis of patients with cervical cancer. Conversely, increased EGFR expression was correlated with poorer survival outcomes, with a higher hazard ratio (HR = 1.6) and a borderline significant p-value (P = 0.055), indicating its possible role as an unfavourable prognostic marker. Additionally, HSP90AA1 expression showed an increased hazard ratio (HR = 1.2), although this relationship was not statistically significant (P = 0.51).

REDVET - Revista electrónica de Veterinaria - ISSN 1695-7504
Vol 25, No. 01 (2024)
http://www.veterinaria.org
Received 07 April 2024 Revised 13 May 2024 Accepted 20 June 2024

In summary, these results demonstrate that among the assessed genes, EGFR and HSP90AA1 may be linked to reduced survival and could be regarded as negative prognostic indicators, whereas AKT1, SRC, STAT3, and TP53 displayed no substantial evidence of overall survival in patients with cervical cancer (Fig 3.6). These results highlight the potential prognostic relevance of EGFR-related pathways in cervical cancer progression and patient outcome.

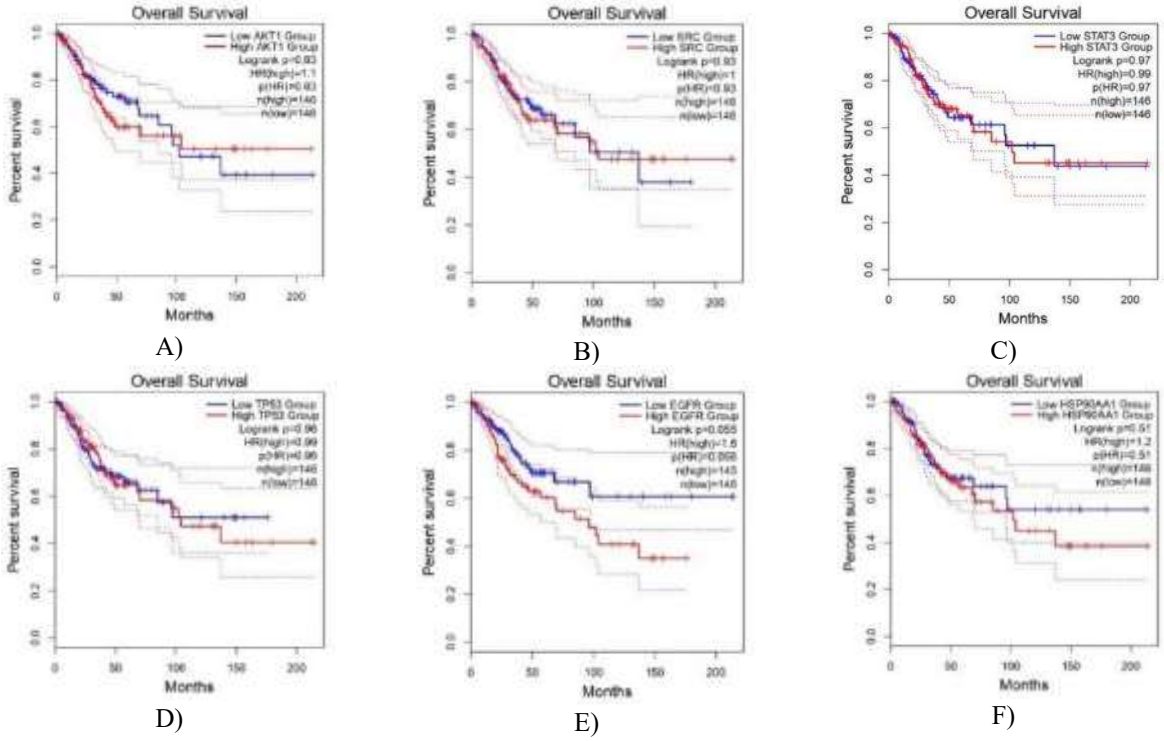

Fig 3.6. Overall survival analyses demonstrating the prognostic significance of cervical cancer–associated hub genes were conducted using Kaplan–Meier survival curves and log-rank tests based on TCGA-CESC (cervical squamous cell carcinoma and endocervical adenocarcinoma) datasets, visualized using GEPIA2. The dashed lines indicate the upper and lower confidence intervals. (a) AKT1 (b) SRC (c) STAT3 (d) TP53 (e) EGFR and (f) HSP90AA1.

Molecular Docking Analysis

6.1.7.1 Molecular Docking with AKT1

The molecular docking analysis for the AKT1 hub protein (PDB ID: 3O96), a central regulator of the PI3K/AKT/mTOR signaling pathway essential for cervical cancer cell survival (10,11), is summarized in Table 3.4. The results revealed that monospermoside exhibited the superior binding affinity with an energy of −9.9 kcal/mol. As illustrated in Fig 3.7, this high-affinity interaction was stabilized by multiple hydrogen bonds with key residues, including TRP-80 (3.08 Å, 3.14 Å), THR-82 (2.33 Å), and THR-211 (2.90 Å).

The second-best binding potential was demonstrated by butin, which recorded a binding energy of −9.6 kcal/mol and established a robust hydrogen bond network with ASN-54 (3.25 Å), GLN-79 (2.00 Å), THR-211 (2.58 Å), VAL-271 (2.12 Å), and TYR-272 (2.63 Å). This was followed by 7,3',4'-trihydroxyflavone, which showed a binding energy of −9.3 kcal/mol and formed a specific hydrogen bond with GLU-79 (2.06 Å). In contrast, coumarin displayed the lowest binding affinity at −6.8 kcal/mol and failed to form any detectable hydrogen bonds. These high-affinity interactions suggest that the chalcones and flavonoids of *B. monosperma* may effectively inhibit AKT1, contributing to the multi-targeted curative potential observed in systems pharmacology models (11,13).

REDVET - Revista electrónica de Veterinaria - ISSN 1695-7504
Vol 25, No. 01 (2024)
http://www.veterinaria.org
Received 07 April 2024 Revised 13 May 2024 Accepted 20 June 2024

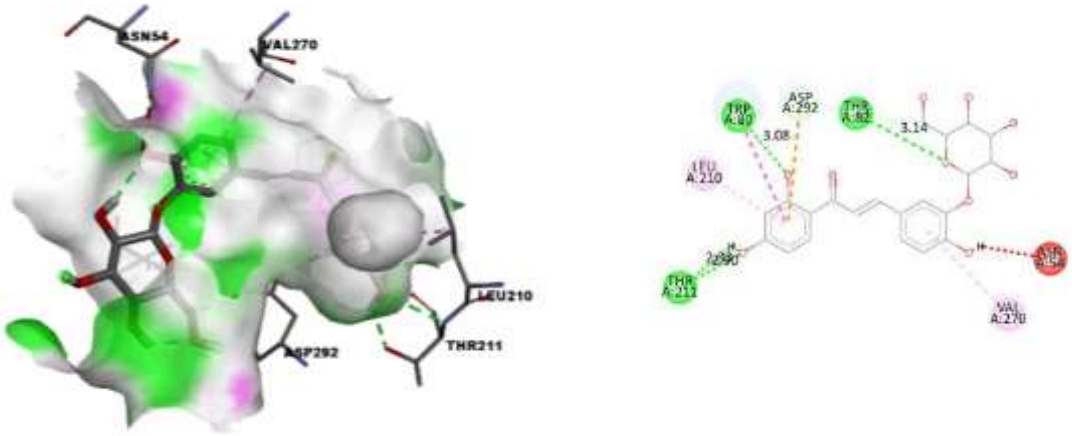

Fig 3.7. Monospermoside and AKT1 docked complex and interaction analysis

6.1.7.2 Molecular Docking Results for TP53 Target

The binding potential of bioactive constituents against the tumor suppressor TP53 (PDB ID: 8DC6), a critical hub gene in the progression of cervical malignancy (13,14), was evaluated and is presented in Table 6.4. Coreopsin emerged as the most potent ligand with a binding affinity of −8.5 kcal/mol. As shown in Fig 3.8, coreopsin's interaction was anchored by an extensive hydrogen bonding network involving residues ARG-10 (3.31 Å), GLN-23 (2.44 Å), ASN-17 (2.67 Å), ILE-21 (2.56 Å), GLU-89 (2.42 Å), ALA-200 (2.13 Å, 2.09 Å), and SER-204 (2.47 Å).

Monospermoside displayed the second-highest binding affinity at −8.3 kcal/mol, establishing critical bonds with ARG-10 (2.99 Å), TYR-92 (2.52 Å), ALA-200 (2.93 Å), and ARG-203 (3.20 Å). Notably, both coreopsin and monospermoside maintained consistent binding energies (−8.5 and −8.3 kcal/mol, respectively) and identical hydrogen bond patterns across different crystal structures, reflecting the high stability and reliability of these protein-ligand interactions (14). These findings support the role of *B. monosperma* phytochemicals in modulating p53-dependent apoptotic pathways as part of a comprehensive anti-cancer strategy (10,13).

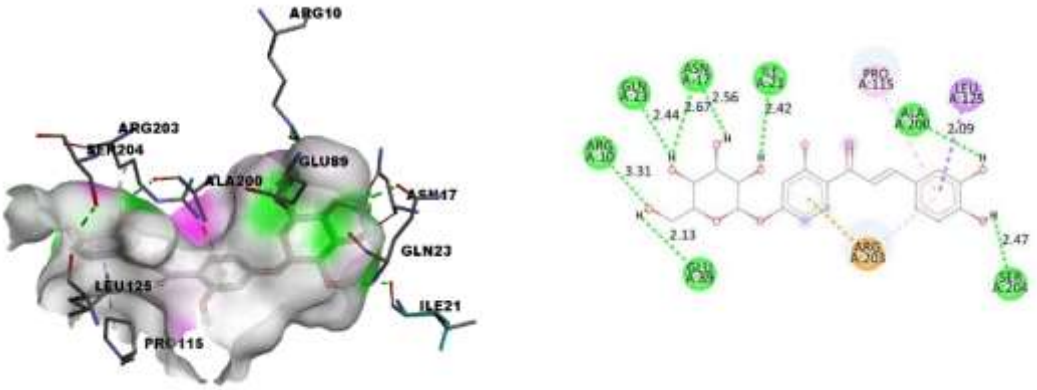

Fig 3.8. Coreosin and TP53 docked complex and interaction analysis

6.1.7.3 Molecular Docking Results for SRC Target

Molecular docking simulations were performed to evaluate the inhibitory potential of *Butea monosperma* flower constituents against the SRC target protein (PDB ID: 2H8H), a non-receptor tyrosine kinase that serves as a critical regulator of cell migration and proliferation in cervical malignancy (9,15). Among the screened phytochemicals identified in this plant (14), isobutrin demonstrated a superior binding affinity of −10.6 kcal/mol, indicating high therapeutic potential. As illustrated in Fig 3.9, this interaction was characterized by an extensive hydrogen bond network involving nine specific residues: CYS-277, LYS-295, VAL-323, THR-338, ARG-388, ASN-391, ASP-404, PHE-405, and THR-416. Other constituents also exhibited significant binding potential; beta-sitosterol showed the second-highest affinity at −9.6 kcal/mol (stabilized by ASP-348), while coreopsin and 7,3',4'-trihydroxyflavone both yielded binding energies of −9.1 kcal/mol. Additionally, butin recorded an affinity of −8.8 kcal/mol, and liquiritigenin displayed a high binding affinity of −8.97 kcal/mol, primarily through hydrophobic interactions. These results, which serve to validate initial

REDVET - Revista electrónica de Veterinaria - ISSN 1695-7504
Vol 25, No. 01 (2024)
http://www.veterinaria.org
Received 07 April 2024 Revised 13 May 2024 Accepted 20 June 2024

network pharmacology predictions, underscore the multi-targeted potential of *B. monosperma* flavonoids in disrupting SRC-mediated oncogenic signaling (5,13).

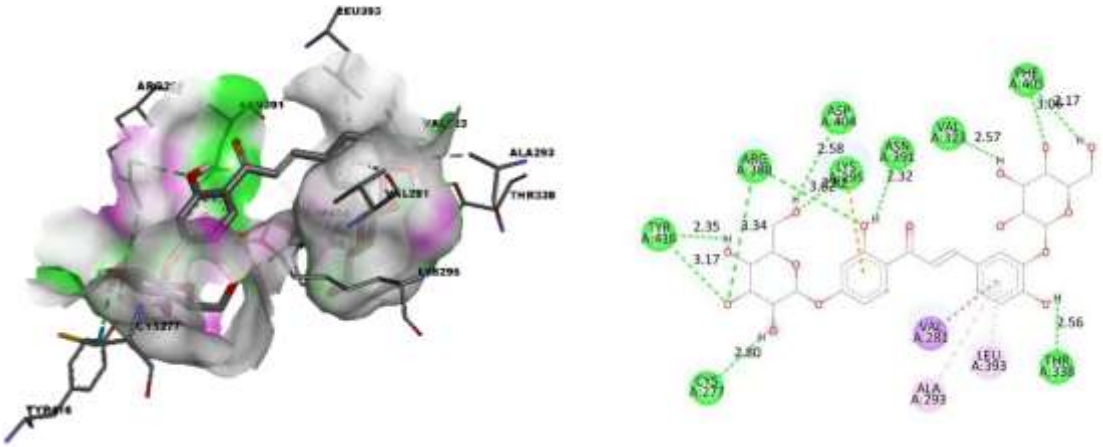

Fig 3.9. Isobutrin and SRC docked complex and interaction analysis

6.1.7.4 Molecular Docking Results for HSP90A Target

The chaperone protein HSP90A (PDB ID: 1BYQ) was targeted to assess the compounds' ability to disrupt the folding and stability of oncogenic client proteins essential for cervical cancer progression (10,14). The docking results, outlined in Table 3.4, identified formononetin as the lead compound with a binding affinity of −7.1 kcal/mol, facilitated by a hydrogen bond with ASN-106 (3.09 Å) (Fig 6.10).

Coreopsin displayed the second-best binding potential at −7.0 kcal/mol, establishing specific hydrogen bonds with ASN-51 (2.34 Å) and PHE-138 (3.08, 3.13 Å). Lower binding energies were observed for afformosin (−5.7 kcal/mol) and coumarin (−5.6 kcal/mol), which interacted with GLY-132/137 and SER-52, respectively.

To evaluate the specificity of these interactions, the affinities of common sugars were also analyzed. D-fructose (−4.7 kcal/mol) and D-glucose (−4.5 kcal/mol) exhibited the weakest binding, despite forming multiple hydrogen bonds with residues like GLU-47, ASN-51, and PHE-138. The significantly higher binding energies of formononetin and coreopsin compared to these primary metabolites suggest that the plant's bioactive flavonoids possess specific inhibitory potential against the HSP90A chaperone system (13,15).

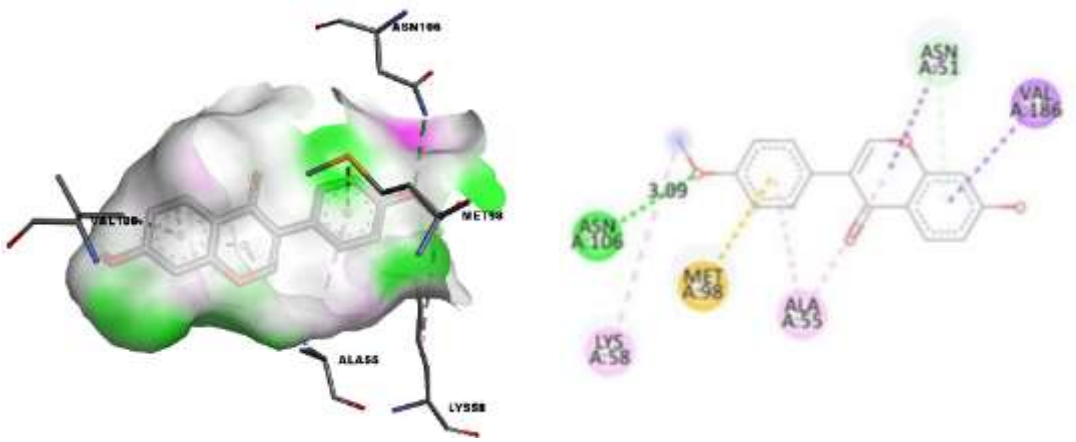

Fig 3.10. Formononetin and HSP90A docked complex and interaction analysis

6.1.7.5 Molecular Docking Results for EGFR Target

The Epidermal Growth Factor Receptor (EGFR, PDB ID: 1XKK) is a critical regulator of cell proliferation and is frequently overexpressed in cervical cancer, positioning it as a primary target for phytochemical-based inhibition (3,4). As summarized in Table 3.4, the molecular docking simulations identified coreopsin and isomonospermoside as having the most significant binding affinities of −9.6 kcal/mol. As illustrated in Fig 3.11, coreopsin established a robust interaction network through multiple hydrogen bonds with LYS-745 (2.83 Å), CYS-775 (2.33 Å), CYS-797 (3.90 Å), and PHE-856 (2.38 Å). Isomonospermoside interacted with SER-720 (2.77 Å), LYS-745 (3.24 Å), and ASP-855 (2.55 Å), as shown in Fig 3.12. Other constituents also demonstrated high binding potential, including monospermoside, which achieved an affinity of −9.4 kcal/mol with hydrogen bonds at CYS-775 and ASN-842, and isobutrin, which reached −9.3 kcal/mol

REDVET - Revista electrónica de Veterinaria - ISSN 1695-7504
Vol 25, No. 01 (2024)
http://www.veterinaria.org
Received 07 April 2024 Revised 13 May 2024 Accepted 20 June 2024

while forming eight distinct hydrogen bonds with residues such as CYS-797, ARG-841, and THR-854. Secondary flavonoids, including liquiritigenin (−8.7 kcal/mol), butein (−8.6 kcal/mol), and isoliquiritigenin (−8.6 kcal/mol), showed consistent affinities; notably, butein has been previously validated for its capacity to suppress cervical cancer growth by modulating the PI3K/AKT/mTOR signaling axis (9). These results suggest that the bioactive constituents of *B. monosperma* flowers may exert their anti-cancer effects by interfering with EGFR-mediated signaling cascades, thereby addressing the dysregulated protein networks characteristic of cervical malignancy (12,13).

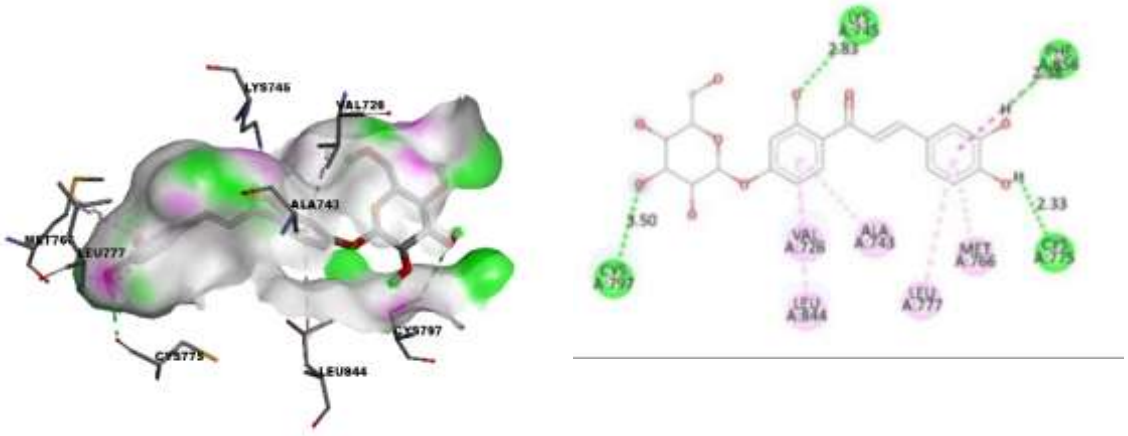

Fig 3.11. Coreopsin and EGFR docked complex and interaction analysis

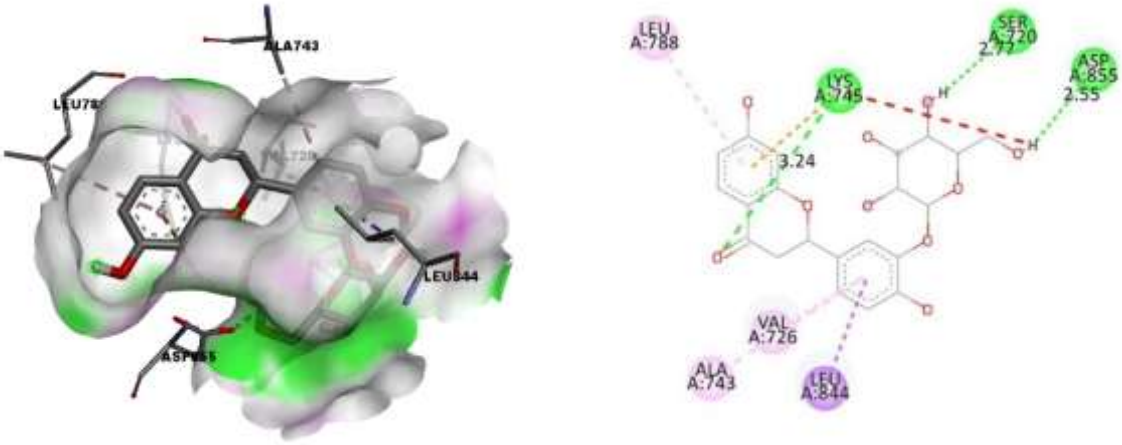

Fig 3.12. Isomonospermoside and EGFR docked complex and interaction analysis

6.1.7.6 Molecular Docking Results for BCL2 Target

To evaluate the potential of these compounds to induce apoptosis, docking was performed against the anti-apoptotic protein BCL2 (PDB ID: 6O0K), a key factor in cancer cell survival (11,13). The results in Table 3.4 show that butrin possessed the highest binding affinity at −8.8 kcal/mol. As depicted in Fig 3.13, it formed several hydrogen bonds with ASP-103 (2.04 Å, 2.31 Å), ASP-111 (2.58 Å), ARG-146 (3.06 Å), and PHE-153 (3.33 Å).

Coreopsin followed closely with an affinity of −8.7 kcal/mol, interacting with ASP-103 and ASP-111. Butin and isoliquiritigenin both recorded affinities of −7.3 kcal/mol, while liquiritigenin and formononetin shared energies of −7.1 kcal/mol. Interestingly, D-glucose (−5.0 kcal/mol) and D-fructose (−4.3 kcal/mol) exhibited significantly lower affinities, highlighting the superior binding efficiency of the plant's secondary metabolites in targeting pro-survival proteins (10,14).

REDVET - Revista electrónica de Veterinaria - ISSN 1695-7504
Vol 25, No. 01 (2024)
http://www.veterinaria.org
Received 07 April 2024 Revised 13 May 2024 Accepted 20 June 2024

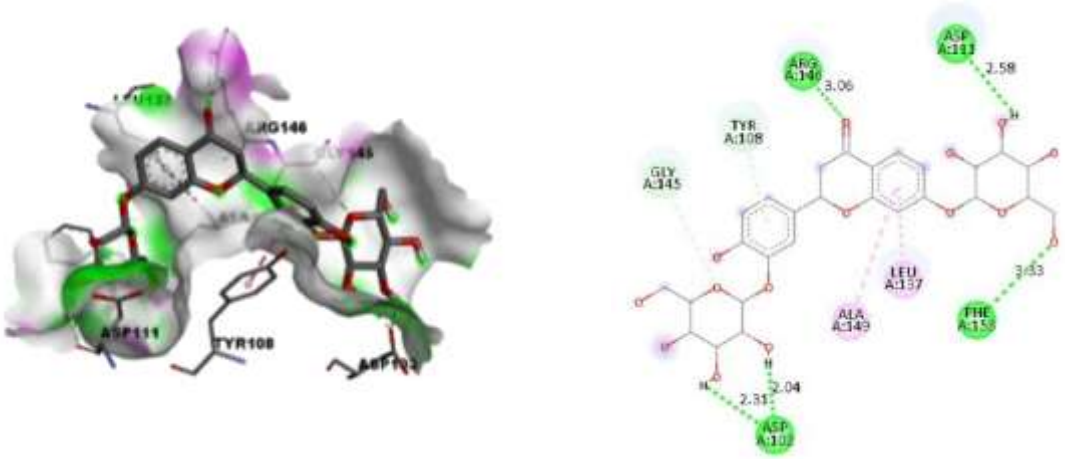

Fig 3.13. Butrin and BCL2 docked complex and interaction analysis

6.1.7.7 Molecular Docking Results for HIF1A Target

The HIF1A protein (PDB ID: 3KCX) is a central mediator of the hypoxic response in solid tumors, contributing to the progression of cervical malignancy (14). Docking results summarized in Table 3.4 identify butin as the top ligand with a binding affinity of −7.9 kcal/mol (Fig 3.14). Although lacking formal hydrogen bonds, the high affinity suggests strong hydrophobic interactions within the binding pocket. Isocoreopsin demonstrated a binding energy of −7.6 kcal/mol, stabilized by bonds with TYR-102, GLN-147, and GLU-202. Coreopsin (−7.2 kcal/mol) displayed the most extensive hydrogen bond network, interacting with GLN-147, THR-196, GLN-203, LYS-214, and ARG-238, indicating its potential to disrupt the stability of the HIF1A complex (13).

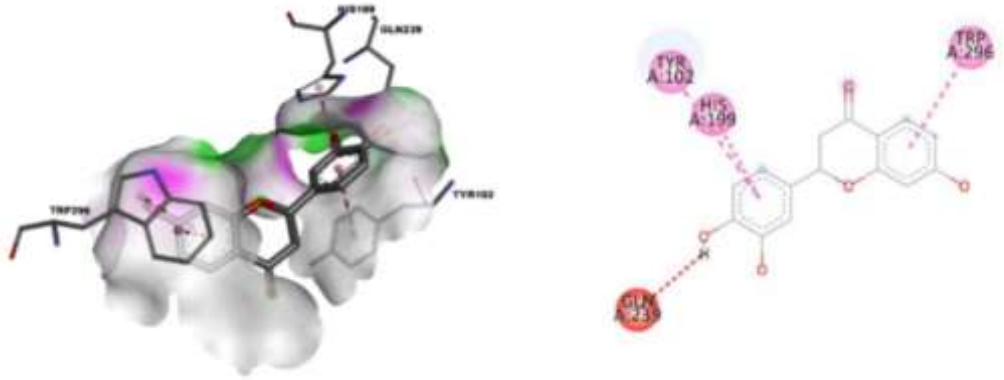

Fig 3.14. Butin and HIF1A docked complex and interaction analysis

6.1.7.8 Molecular Docking Results for HSP90AB1 Target

Docking analysis for the molecular chaperone HSP90AB1 (PDB ID: 3NMQ), which maintains the stability of oncogenic client proteins (14), revealed that formononetin exhibited the best binding affinity at −9.6 kcal/mol. As shown in Fig 3.15, it formed hydrogen bonds with ASP-93 (1.97 Å) and TYR-139 (2.98 Å). Coreopsin followed with a binding energy of −9.2 kcal/mol, interacting with ASN-51, ASP-102, and GLY-108. Monospermoside also showed high affinity (−9.1 kcal/mol), while the long-chain fatty acid tetracosanoic acid showed the weakest binding at −6.6 kcal/mol. These results underscore the potential of *B. monosperma* flowers to inhibit the chaperone systems required for tumor growth (10,13).

REDVET - Revista electrónica de Veterinaria - ISSN 1695-7504
Vol 25, No. 01 (2024)
http://www.veterinaria.org
Received 07 April 2024 Revised 13 May 2024 Accepted 20 June 2024

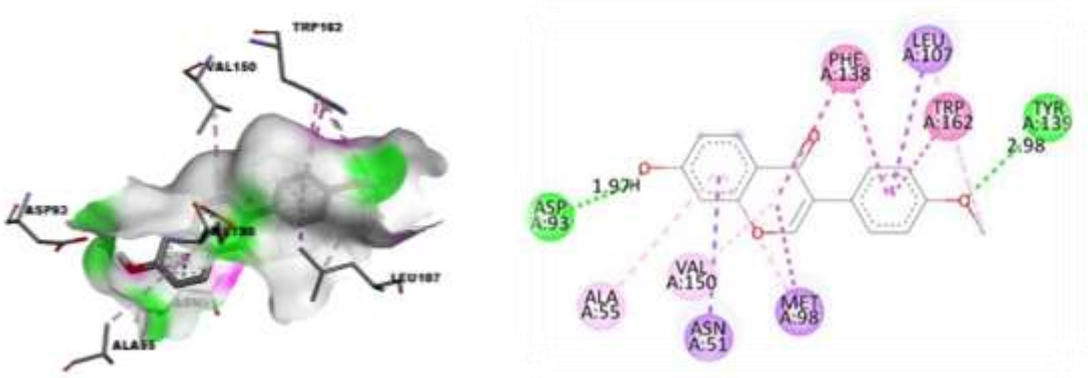

Fig. 3.15. Formononetin and HSP90AB1 docked complex and interaction analysis

6.1.7.9 Molecular Docking Results for TNF Target

Finally, the inflammatory cytokine TNF (PDB ID: 2AZ5), a major component of the tumor microenvironment (15), was analyzed. Isocoreopsin and sulfurein shared the highest binding affinity of −8.3 kcal/mol. As illustrated in Fig 3.16 and 3.17, isocoreopsin interacted with GLY-121 and TYR-151, while sulfurein established bonds with PRO-117, TYR-119, and GLY-121. Coreopsin (−7.9 kcal/mol) and isobutrin (−7.8 kcal/mol) also demonstrated extensive interaction profiles involving both the A and B chains of the TNF dimer. The significant binding of these phytochemicals suggests they may modulate the inflammatory landscape of cervical tumors (13,15).

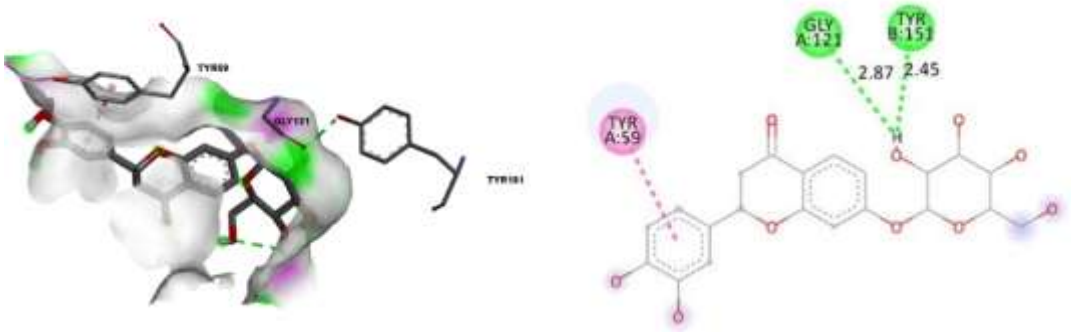

Fig. 3.16. Isocoreopsin and TNF docked complex and interaction analysis

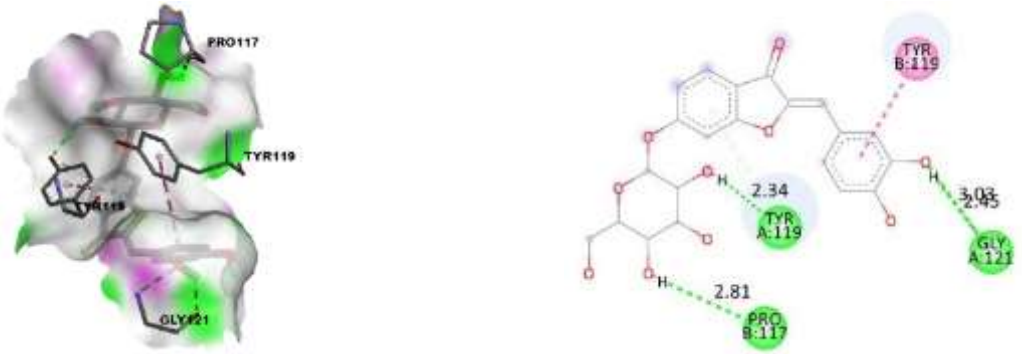

Fig. 3.17. Sulfurein and TNF docked complex and interaction analysis

REDVET - Revista electrónica de Veterinaria - ISSN 1695-7504
Vol 25, No. 01 (2024)
http://www.veterinaria.org
Received 07 April 2024 Revised 13 May 2024 Accepted 20 June 2024

Table 3.4: Summary of molecular docking results of *B. monosperma* flowers against the selected target proteins.

Molecular name	Targets	PDB ID	Residue involved in H bonding	H-bond length (Å)	Binding energy (kcal/Mol)
7,3',4'-trihydroxyflavone	AKT1	3O96	GLU-79	2.06	-9.3
Monospermoside	AKT1	3O96	TRP-80;THR-82;THR-211	3.08;3.14;2.33;2.90	-9.9
Coumarin	AKT1	3O96	-	-	-6.8
Butin	AKT1	3O96	ASN-54;GLN-79;THR-211;VAL-271;TYR-272	3.25;2.00;2.58;2.12;2.63	-9.6
Coreopsin	TP53	8DC6	ARG-10;GLN-23;ASN-17;ILE-21;GLU-89;ALA-200;SER-204	3.31;2.44;2.67;2.56;2.42;2.13;2.09;2.47	-8.5
Monospermoside	TP53	8DC6	ARG-10;TYR-92;ALA-200;ARG-203	2.99;2.52;2.93;3.20	-8.3
Butin	SRC	2H8H	ALA-390;ASN-391;ASP-404	2.56;2.10;3.38	-8.8
Coreopsin	SRC	2H8H	ASP-348;THR-338	2.23;2.59;3.13	-9.1
Coumarin	SRC	2H8H	THR-338	3.25	-7
Isobutrin	SRC	2H8H	CYS-277;LYS-295;VAL-323;THR-338;ARG-388;ASN-391;ASP-404;PHE-405;THR-416	2.80;2.82;2.57;2.56;3.34;3.02;2.32;2.58;2.17;3.06;2.35;3.17	-10.6
Beta Sitosterol	SRC	2H8H	ASP-348	2.31	-9.6
Isoliquiritigenin	SRC	2H8H	MET-341	3.23	-8.3
Liquiritigenin	SRC	2H8H	-	-	-8.9
7,3',4'-trihydroxyflavone	SRC	2H8H	THR-338;MET-341	3.22;3.02	-9.1
Coreopsin	HSP90A	1BYQ	ASN-51;PHE-138	2.34;3.08;3.13	-7
Coumarin	HSP90A	1BYQ	SER-52	2.85	-5.6
D-Glucose	HSP90A	1BYQ	GLU-47;GLY-135;PHE-138	2.59;1.93;2.37;3.02	-4.5
D-Fructose	HSP90A	1BYQ	GLU-47;ASN-51;PHE-138	2.15;2.08;3.21	-4.7
Formononetin	HSP90A	1BYQ	ASN-106	3.09	-7.1
Afrormosin	HSP90A	1BYQ	GLY-132;GLY-137	2.76;2.90	-5.7
D-Glucose	STAT3	6NJS	ARG-609;SER-613	2.83;2.90;3.09	-4.9
D-Fructose	STAT3	6NJS	ARG-609;SER-611;GLU-612;SER-613;THR-620	3.00;2.92;3.06;2.99;3.06;3.00;2.90	-4.4
Coreopsin	EGFR	1XKK	LYS-745;CYS-775;CYS-797;PHE-856	2.83;2.33;3.90;2.38	-9.6
Isomonospermoside	EGFR	1XKK	SER-720;LYS-745;ASP-855	2.77;3.24;2.55	-9.6
Monospermoside	EGFR	1XKK	CYS-775;ASN-842	2.60;1.99	-9.4
Coumarin	EGFR	1XKK	THR-854	2.97	-6.7
Butein	EGFR	1XKK	MET-766	2.07	-8.6

REDVET - Revista electrónica de Veterinaria - ISSN 1695-7504
Vol 25, No. 01 (2024)
http://www.veterinaria.org
Received 07 April 2024 Revised 13 May 2024 Accepted 20 June 2024

Isobutrin	EGFR	1XKK	CYS-775;CYS-797;ARG-841;ASN-842;THR-854;ASP-855;PHE-856	2.12;3.54;2.80;2.88;3.11;2.15;2.55;2.02;2.97	-9.3
Isoliquiritigenin	EGFR	1XKK	MET-766;ASP-855	2.13;2.97	-8.6
7,3',4'-trihydroxyflavone	EGFR	1XKK	MET-793	3.26;2.80	-8.8
Liquiritigenin	EGFR	1XKK	MET-793	2.74;3.12	-8.7
Formononetin	EGFR	1XKK	-	-	-8.4
Afrormosin	EGFR	1XKK	CYS-797	3.01	-8.1
Tetracosanoic acid	BCL2	6O0K	-	-	-6
Coreopsin	BCL2	6O0K	ASP-103;ASP-111	1.79;2.93	-8.7
Butrin	BCL2	6O0K	ASP-103;ASP-111;ARG-146;PHE-153	2.04;2.31;2.58;3.06;3.33	-8.8
Butin	BCL2	6O0K	PHE-153	3.1	-7.3
Isocoreopsin	BCL2	6O0K	-	-	
D Glucose	BCL2	6O0K	ALA-149	2.12;2.49	-5
D-Fructose	BCL2	6O0K	-	-	-4.3
Isoliquiritigenin	BCL2	6O0K	ASP-103	2.14	-7.3
Liquiritigenin	BCL2	6O0K	-	-	-7.1
Formononetin	BCL2	6O0K	-	-	-7.1
Afrormosin	BCL2	6O0K	ARG-146	3.16	-6.8
Tetracosanoic acid	HIF1A	3KCX	ARG-238	2.87	-5.9
Coreopsin	HIF1A	3KCX	GLN-147;THR-196;GLN-203;LYS-214;ARG-238	2.98;2.91;2.84;3.22;3.03;2.95;3.20	-7.2
Butrin	HIF1A	3KCX	TYR-102;TYR-145;THR-196;ARG-238	3.07;1.96;2.44;2.93	-2.9
Butin	HIF1A	3KCX	-	-	-7.9
Isocoreopsin	HIF1A	3KCX	TYR-102;GLN-147;GLU-202	3.15;2.80;3.14;3.03	-7.6
Coreopsin	TP53	3DCY	ARG-10;ASN-17;ILE-21;GLN-23;GLU-89;ALA-200;SER-204	3.31;2.67;2.56;2.42;2.44;2.13;2.09;2.47	-8.5
Monospermoside	TP53	3DCY	ARG-10;TYR-92;ALA-200;ARG-203	2.99;2.52;2.93;3.20	-8.3
Tetracosanoic acid	HSP90AB1	3NMQ	ALA-52	3.21	-6.6
Coreopsin	HSP90AB1	3NMQ	ASN-51;ASP-102;GLY-108;	2.96;2.48;2.86	-9.2
Monospermoside	HSP90AB1	3NMQ	GLY-97;THR-184	2.30;3.08	-9.1
Formononetin	HSP90AB1	3NMQ	ASP-93;TYR-139	1.97;2.98	-9.6
Tetracosanoic acid	TNF	2AZ5	-	-	-5.3
Coreopsin	TNF	2AZ5	GLYA-121;TYRA-151;SERB-60;TYRB-151	2.21;2.94;2.68;3.33;2.45	-7.9

REDVET - Revista electrónica de Veterinaria - ISSN 1695-7504
Vol 25, No. 01 (2024)
http://www.veterinaria.org
Received 07 April 2024 Revised 13 May 2024 Accepted 20 June 2024

Isobutrin	TNF	2AZ5	SERA-60;TYRA-119;SERB;60;PROB-117;TYRB-119;LEUB-120;TYRB-151	2.73;2.55;2.63;2.25;3.30;1.86;3.01;3.30	-7.8
Isocoreopsin	TNF	2AZ5	GLYA-121;TYRB-151	2.87;2.45	-8.3
Sulfurein	TNF	2AZ5	PRO-117;TYR-119;GLY-121	2.81;2.34;2.45;3.03	-8.3
formononetin	TNF	2AZ5	SER B-60;TYR B-151	2.76;3.17	-7.6
Afformosin	TNF	2AZ5	-	-	-7

6.1.8 Molecular Dynamics Simulations

To validate the thermodynamic stability and conformational flexibility of the prioritized protein-ligand complexes, Molecular Dynamics simulations were performed. These simulations are essential for confirming that the predicted binding interactions remain consistent under physiological-like conditions, supporting the multi-targeted curative potential of *Butea monosperma* flowers (10,13).

6.1.8.1 MD Simulation of the Monospermoside-AKT1 Complex and RMSF Analysis

The stability of the monospermoside-AKT1 docked complex (PDB ID: 3O96) was evaluated using Normal Mode Analysis, which revealed moderate peaks in the main chain deformability graph and identified flexible hinge regions that facilitate conformational adjustments upon ligand binding (Fig 3.18). B-factor analysis demonstrated a high degree of correlation between the NMA-derived fluctuations and experimental PDB data, confirming the structural reliability of the simulated model. Key dynamic parameters included a low eigenvalue of (3.2×10^{-4}) and an individual variance of approximately 18% for the primary modes; this low eigenvalue indicates reduced structural stiffness, suggesting that the monospermoside-AKT1 interaction is energetically favorable and highly stable. Further analysis through a covariance map and elastic network graph reflected coordinated dynamics and low stiffness, indicating that the AKT1 protein effectively accommodates monospermoside through localized deformation.

To assess residue-level flexibility, Root Mean Square Fluctuation analysis was conducted using the CABS-flex 2.0 server, showing that critical interacting residues—including LYS-30, THR-81, THR-82, LYS-158, LEU-202, GLY-204, VAL-206, ALA-230, MET-281, and PHE-383—exhibited significantly reduced fluctuations (RMSF < 1.5 Å) in the bound state. This rigidification of the binding pocket confirms the formation of a stable complex, which is expected to inhibit the AKT1 signaling axis. Because the PI3K/AKT/mTOR pathway is a central regulator of survival and proliferation in cervical cancer, the stable binding of *Butea monosperma* constituents to AKT1 represents a significant therapeutic mechanism for inducing apoptosis and growth arrest (9). This target-specific stability supports the broader polypharmacological potential of the plant's bioactive flavonoids in addressing the dysregulated protein networks of cervical malignancy (9,14).

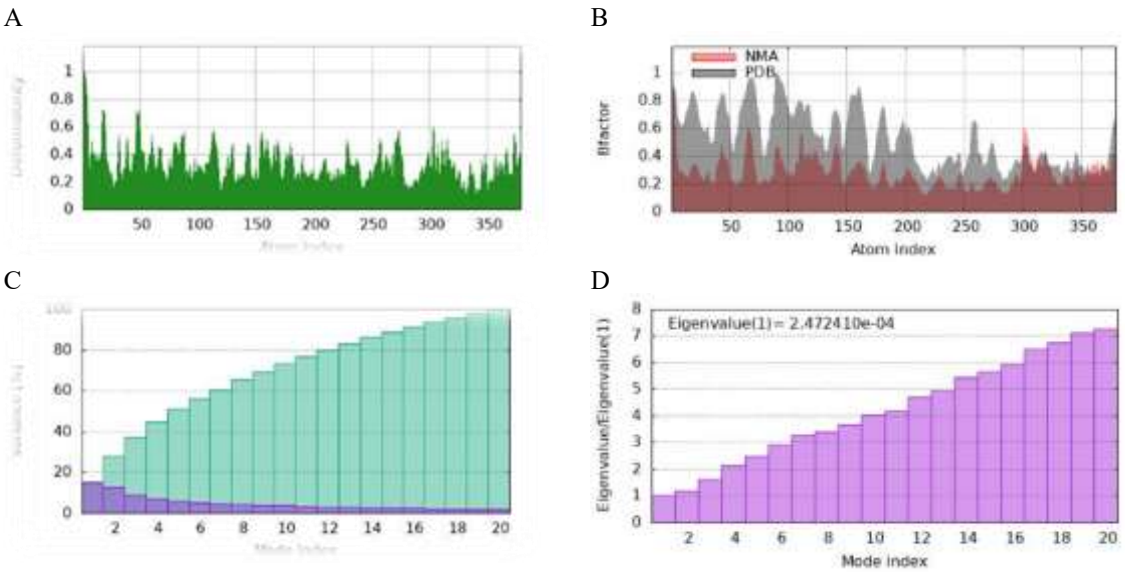

REDVET - Revista electrónica de Veterinaria - ISSN 1695-7504
Vol 25, No. 01 (2024)
http://www.veterinaria.org
Received 07 April 2024 Revised 13 May 2024 Accepted 20 June 2024

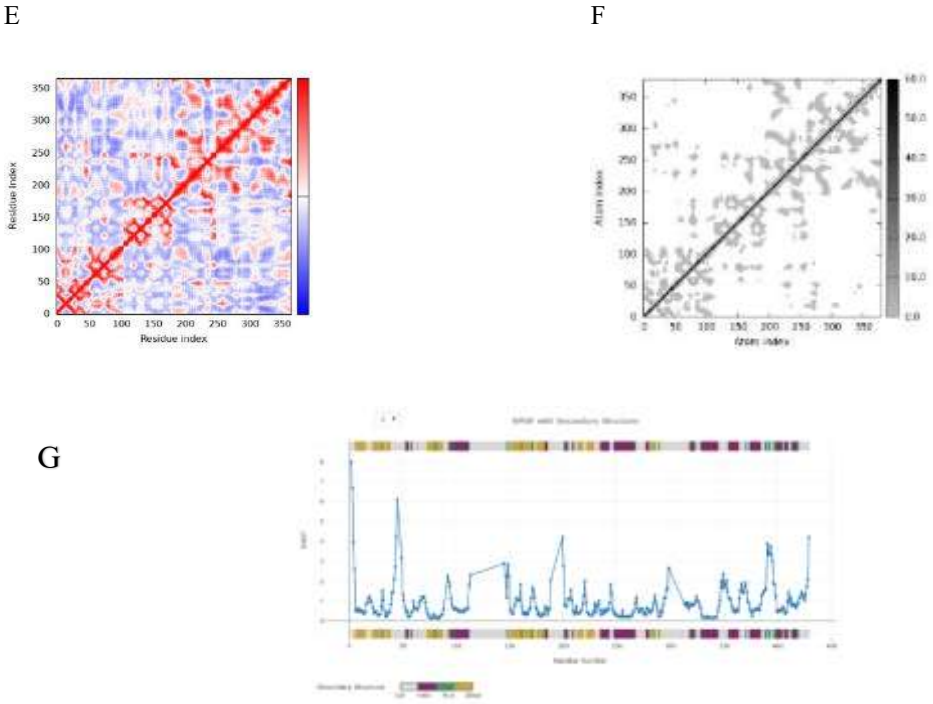

Fig. 3.18. MD simulation output for Monospermoside-AKT1 docked complex: (A) Deformability; (B) B-factor; (C) Variance; (D) Eigenvalue; (E) Covariance map; (F) Elastic network model; (G) RMSF Analysis of the Monospermoside–AKT1 Complex (CABS-flex 2.0) (protein rigidity: 1.0, number of cycles: 50, cycle between trajectory: 50 for the 10 ns) of CABS Flex 3.0 server

6.1.8.2 MD Simulation of the Isobutrin-SRC Complex and RMSF Analysis

The dynamic stability of the isobutrin-SRC complex (PDB ID: 2H8H) was scrutinized using Normal Mode Analysis, identifying medium-to-high flexibility across the structure with distinct hinge regions that facilitate the interaction between the SRC kinase domain and the isobutrin ligand (Fig 3.19). The B-factor plot displayed a consistent peak pattern between the NMA simulation and experimental PDB data, further validating the accuracy of the simulated model. Statistical analysis revealed an exceptionally low eigenvalue of 9.149730e-05, corresponding to an individual variance of approximately 20%, which indicates that the complex is both structurally robust and functionally flexible, requiring minimal energy for necessary conformational changes.

The covariance map exhibited strong coupling between residue pairs, while the elastic network model suggested high flexibility at the binding interface, characterized by dominant light-grey regions. Furthermore, Root Mean Square Fluctuation analysis of the SRC kinase confirmed that residues within the ATP-binding site and hinge region (residues 270–420) underwent significant rigidification upon isobutrin binding, with RMSF values falling below 1.5 Å. In contrast, the distal SH2 and SH3 domains maintained their inherent mobility with fluctuations exceeding 3–4 Å. These findings strongly support the stability of the isobutrin-SRC interaction and highlight isobutrin, a key constituent of *Butea monosperma* (14), as a potent modulator of SRC-mediated oncogenic pathways in cervical cancer. By stabilizing such critical nodes, these phytochemicals likely disrupt the dysregulated protein networks—including the PI3K/AKT/mTOR axis—that drive cervical malignancy (9,13).

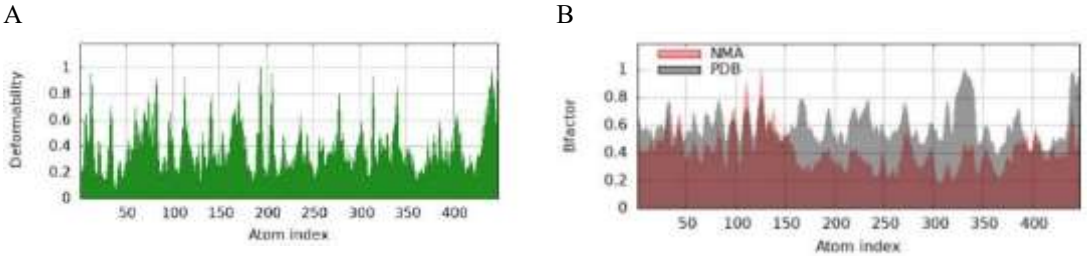

REDVET - Revista electrónica de Veterinaria - ISSN 1695-7504
Vol 25, No. 01 (2024)
http://www.veterinaria.org
Received 07 April 2024 Revised 13 May 2024 Accepted 20 June 2024

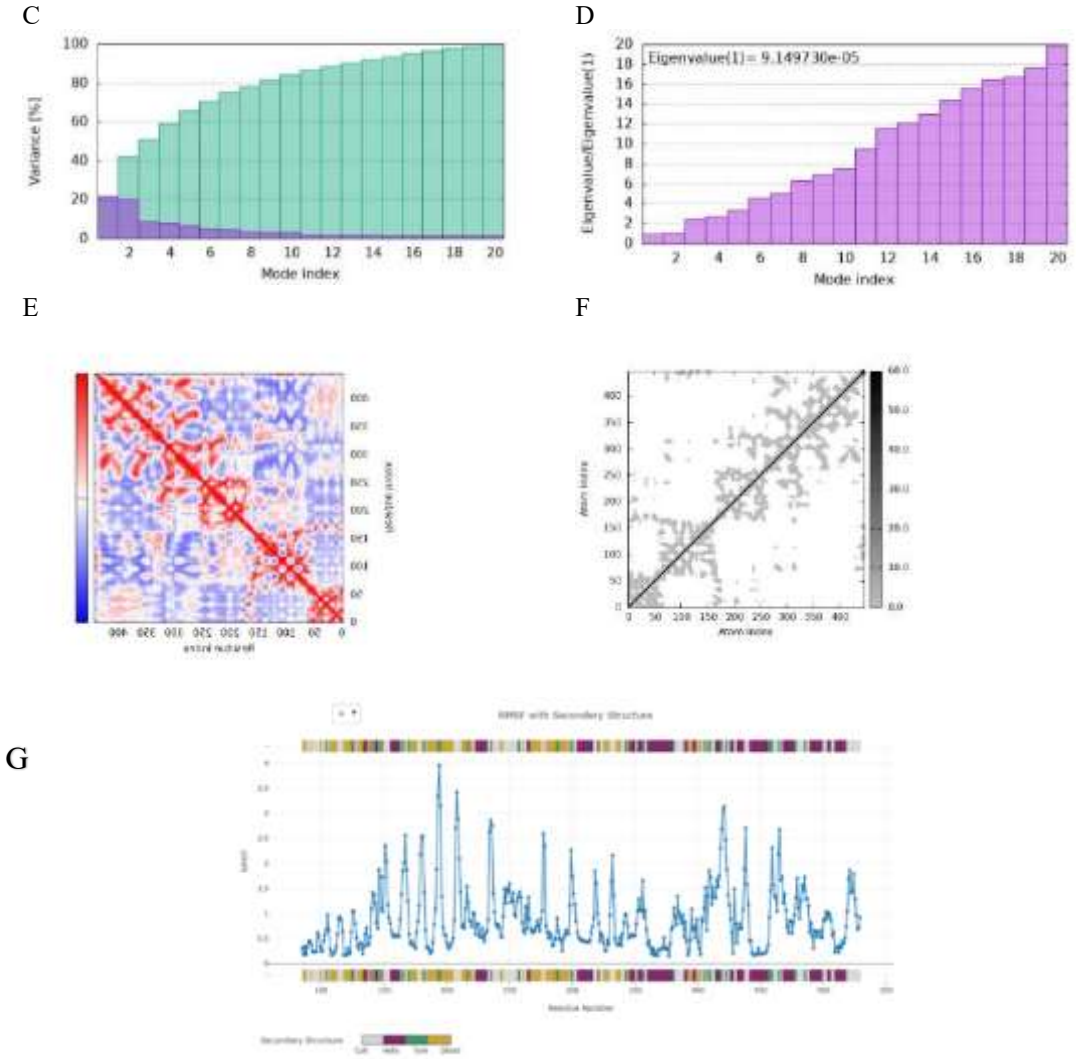

Fig. 3.19. MD simulation output for Isobutrin-SRC docked complex: (A) Deformability; (B) B-factor; (C) Variance; (D) Eigenvalue; (E) Covariance map; (F) Elastic network model (G) RMSF Analysis of the Isobutrin-SRC docked Complex (CABS-flex 2.0) (protein rigidity: 1.0, number of cycles: 50, cycle between trajectory: 50 for the 10 ns) of CABS Flex 3.0 server

Discussion

Cervical cancer persists as a formidable global health challenge, ranking as the fourth most common cause of cancer-related mortality among women worldwide (11). In 2022, approximately 662,044 new cases and 348,709 deaths were recorded globally, with a disproportionate burden falling on low- and middle-income countries like India (4,11). The complexity of its pathogenesis, primarily driven by high-risk HPV genotypes and co-factors like smoking and poor nutrition, necessitates the exploration of multi-targeted therapies that can address dysregulated protein networks more effectively than conventional "one-target" approaches (12,13).

Our PPI network analysis identified AKT1, SRC, EGFR, and TP53 as primary regulatory hubs, which is consistent with their established roles as central inducers of cervical carcinogenesis (9,18). Specifically, AKT1 acts as a critical node in the PI3K/Akt signaling cascade that governs cell survival and proliferation; in HPV-positive cervical cancer, the interplay of various microRNAs with the PI3K-AKT axis serves as a key diagnostic signal and putative regulatory target (9,19). Furthermore, SRC has been identified as a major driver of tumorigenesis and drug resistance in cervical cancer, where its activation promotes downstream signaling pathways essential for tumor progression (18,20). The identification of TP53 and BCL2 as hubs aligns with previous findings identifying these genes as essential for diagnostic and therapeutic targeting in gynecological malignancies (7,15). Our docking results, showing high binding affinities of *B. monosperma* flower constituents like isobutrin (−10.6 kcal/mol) toward these hubs, suggest that these phytochemicals can effectively disrupt the oncogenic signaling required for tumor progression (3,5).

The therapeutic efficacy of *B. monosperma* flowers is likely driven by its rich profile of chalcones and flavonoids, particularly butein, butrin, and isobutrin (6,14). Butein is characterized as a potent anti-cancer agent that suppresses

cervical cancer growth by inducing G2/M phase cell cycle arrest through the inhibition of the PI3K/AKT/mTOR pathway (9). Beyond this axis, butein has also been shown to inhibit cell growth by blocking the IL-6/IL-6Rα interaction and regulating the IL-6/STAT3/FoxO3a pathway, highlighting its versatile polypharmacological potential (10). Our docking analysis further elucidates this mechanism, showing that butein and its derivatives form stable hydrogen bond networks with key residues in the AKT1 and EGFR kinase domains (3,9).

A critical hallmark of effective cancer therapy is the restoration of apoptotic pathways. The modulation of the Bcl-2/Bax ratio is a primary mechanism through which *B. monosperma* flower constituents exert their pro-apoptotic effects (9,15). Specifically, butein treatment leads to the upregulation of pro-apoptotic markers and the downregulation of cell survival genes like AKT and mTOR (9). Furthermore, the generation of reactive oxygen species mediates butein-induced apoptosis, a mechanism observed in various cancer models to trigger programmed cell death (16). By stabilizing TP53 and inhibiting anti-apoptotic proteins like BCL2, these bioactive molecules effectively license cell death in malignant cells (15,16).

Molecular Dynamics simulations provided essential evidence that the prioritized protein-ligand complexes remain stable under physiological conditions (5,12). The low eigenvalues observed for the monospermoside-AKT1 (3.2×10^{-4}) and isobutrin-SRC ($9.15x10^{-5}$) complexes indicate high energetic stability and reduced structural stiffness, which are critical for sustained therapeutic activity (5). Furthermore, the RMSF analysis showing rigidification of the binding pockets (< 1.5 Å) confirms that these phytochemicals occupy the active sites of their targets with high residence times, a finding supported by similar structural studies of other potent kinase inhibitors (13,17). This stability is vital for the sustained inhibition of signaling hubs like EGFR and SRC, which are pivotal for mediating resistance to conventional therapies (3,18).In summary, this integrated systems pharmacology study reveals that *Butea monosperma* acts through a sophisticated "multi-compound, multi-target" mechanism to combat cervical cancer. By simultaneously targeting proliferative signaling (EGFR, AKT1, SRC) and inducing apoptosis (BCL2, TP53), these phytochemicals offer a robust therapeutic strategy (9,13). These findings validate the traditional medicinal use of *B. monosperma* and provide a rigorous computational foundation for future *in vitro* and *in vivo* validation in the quest for safer and more effective cervical cancer treatments (5,12).

References

1. Jouya S, Shahabinia Z, Mazidimoradi A, Allahqoli L, Salehiniya H, Lee DY. Cervical Cancer Epidemiology: Global Incidence, Mortality, Survival, Risk Factors, and Equity in HPV Screening and Vaccination. Journal of Clinical Medicine [Internet]. 2026 Jan 29 [cited 2026 Feb];15(3):1079. Available from: https://doi.org/10.3390/jcm15031079
2. Ma Y, Lai X, Fang H. Global, regional, and national disease burden and economic costs of cervical cancer (1991–2021): a multidimensional data synthesis analysis. Frontiers in Public Health [Internet]. 2025 Sep 11 [cited 2025 Oct];13. Available from: https://doi.org/10.3389/fpubh.2025.1633975
3. Huang S, Wang R, Song Y, Liao SM, Ou M, Huang Y, et al. Uncovering the anti-cervical cancer mechanism of Ziyuglycoside I via integrated network pharmacology molecular docking and experimental validation. Scientific Reports [Internet]. 2025 Oct 16 [cited 2025 Oct];15(1). Available from: https://doi.org/10.1038/s41598-025-20129-z
4. Zhou J, Li H, Wu B, Zhu L, Huang Q, Guo Z, et al. Network pharmacology combined with experimental verification to explore the potential mechanism of naringenin in the treatment of cervical cancer. Scientific Reports [Internet]. 2024 Jan 22 [cited 2025 Oct];14(1). Available from: https://doi.org/10.1038/s41598-024-52413-9
5. Bhattacharya K, Nath BC, Ahmed E, Khanal P, Chanu NR, Deka S, et al. Integration of network pharmacology, molecular docking, and simulations to evaluate phytochemicals from Drymaria cordata against cervical cancer. 2024 Jan 1 [cited 2025 Oct]; Available from: https://doi.org/10.1039/d3ra06297j
6. Jain S, Dubey PK. Butea monosperma (Lam.) Taub: Review on its chemistry, morphology, ethnomedical uses, phytochemistry and pharmacological activities. Journal of Drug Delivery and Therapeutics [Internet]. 2023 Apr 15 [cited 2025 Oct];13(4):137. Available from: https://doi.org/10.22270/jddt.v13i4.5782
7. Dua R, Bhardwaj T, Ahmad I, Somvanshi P. Investigating the potential of Juglans regia phytoconstituents for the treatment of cervical cancer utilizing network biology and molecular docking approach. 2024 Apr 16 [cited 2025 Oct]; Available from: https://doi.org/10.1371/journal.pone.0287864
8. Aarthy M, Muthuramalingam P, Ramesh M, Singh SK. Unraveling the multi-targeted curative potential of bioactive molecules against cervical cancer through integrated omics and systems pharmacology approach. 2022 Aug 21 [cited 2025 Oct]; Available from: https://doi.org/10.1038/s41598-022-18358-7
9. Bai X, Ma Y, Zhang G. Butein suppresses cervical cancer growth through the PI3K/AKT/mTOR pathway. 2015 Apr 24 [cited 2025 Aug]; Available from: https://doi.org/10.3892/or.2015.3922
10. Park S, Seo YJ, Kim LK, Kim HJ, Yoon KD, Heo T. Butein Inhibits Cell Growth by Blocking the IL-6/IL-6Rα Interaction in Human Ovarian Cancer and by Regulation of the IL-6/STAT3/FoxO3a Pathway. 2023 Mar 23 [cited 2026 Mar]; Available from: https://doi.org/10.3390/ijms24076038
11. Wu J, Jin Q, Zhang Y, Ji Y, Li J, Liu X, et al. Global burden of cervical cancer: current estimates, temporal trend and future projections based on the GLOBOCAN 2022. 2025 Jan 23 [cited 2025 Nov]; Available from: https://doi.org/10.1016/j.jncc.2024.11.006

12. Kamau SW, Jepkorir M, Kipkoech G, Lagu IJL, Kanda W, Kibunja S, et al. Antiproliferative activity of Grewia villosa ethyl acetate extract on cervical cancer HeLa cell line: Mechanistic insights through network pharmacology and functional assays approach. PLoS ONE [Internet]. 2025 Sep 24 [cited 2025 Sep];20(9). Available from: https://doi.org/10.1371/journal.pone.0331649
13. Yuan Z, Pan Y, Leng T, Yu C, Zhang H, Ma J, et al. Progress and Prospects of Research Ideas and Methods in the Network Pharmacology of Traditional Chinese Medicine. Journal of Pharmacy & Pharmaceutical Sciences [Internet]. Canadian Society for Pharmaceutical Sciences; 2022 Jun 21 [cited 2025 Oct];25:218. Available from: https://doi.org/10.18433/jpps32911
14. MT M, Ranjith D, Yaligar R, Jyothi R, Narappa G, Mv R. Swiss ADME prediction of phytochemicals present in Butea monosperma (Lam.) Taub. Journal of Pharmacognosy and Phytochemistry [Internet]. 2020 Jan 1 [cited 2025 Oct];9(3):1799. Available from: https://www.phytojournal.com/archives/2020/vol9issue3/PartAD/9-3-296-345.pdf
15. Yang P, Hu D, Kao YH, Lin I, Liu F. Butein induces apoptotic cell death of human cervical cancer cells. Oncology Letters [Internet]. 2018 Sep 7 [cited 2025 Sep]; Available from: https://doi.org/10.3892/ol.2018.9426
16. Chen Y, Yeh C, Lo H, Su S, Hseu Y, Hsu L. Generation of reactive oxygen species mediates butein-induced apoptosis in neuroblastoma cells. Oncology Reports [Internet]. 2012 Jan 12 [cited 2025 Jul];27(4):1233. Available from: https://doi.org/10.3892/or.2012.1632
17. Ralte L, Sailo H, Kumar R, Khiangte L, Kumar NS, Singh YT. Identification of novel AKT1 inhibitors from Sapria himalayana bioactive compounds using structure-based virtual screening and molecular dynamics simulations. BMC Complementary Medicine and Therapies [Internet]. 2024 Mar 7 [cited 2025 Oct];24(1). Available from: https://doi.org/10.1186/s12906-024-04415-3
18. Kong L, Deng Z, Shen H, Zhang Y. Src family kinase inhibitor PP2 efficiently inhibits cervical cancer cell proliferation through down-regulating phospho-Src-Y416 and phospho-EGFR-Y1173. Molecular and Cellular Biochemistry [Internet]. 2010 Nov 3 [cited 2026 Jan];348:11. Available from: https://doi.org/10.1007/s11010-010-0632-1
19. Rahimi-Moghaddam A, Ghorbanmehr N, Gharbi S, Nili F, Korsching E. Interplay of miR-542, miR-126, miR-143 and miR-26b withPI3K-AKT is a diagnostic signal and putative regulatory target in HPV-Positive Cervical Cancer. Research Square (Research Square) [Internet]. 2024 Jan 5 [cited 2025 Sep]; Available from: https://doi.org/10.21203/rs.3.rs-3831690/v1
20. Meng M, Guo Y, Chen Y, Li X, Zhang B, Xie Z, et al. Cancer/testis-45A1 promotes cervical cancer cell tumorigenesis and drug resistance by activating oncogenic SRC and downstream signaling pathways. Cellular Oncology [Internet]. 2023 Nov 4 [cited 2025 Aug];47(2):657. Available from: https://doi.org/10.1007/s13402-023-00891-w